Effect of Square Pin Tool on Friction Stir Welded AA 6061-T6 from the Perspective of Revolution Pitch

Abhijit Banik[1] , Tapas Debnath[2] , John Deb Barma[3] , Subhash Chandra Saha[3§]

[1] NIT Mizoram, Faculty, Department of Mechanical Engineering, Aizwal, Mizoram, India.
[2] Karunya Institute of Technology and Science, Department of Mechanical Engineering, Coimbatore, Tamil Nadu, India.
[3] NIT Agartala, Department of Mechanical Engineering, Agartala, Tripura, India.
[§]Professor (Retired).

Abstract: The phenomenon of revolution pitch was studied on AA 6061-T6 with a square pin tool for friction stir welding (FSW). The tool rotational speed and traverse speed were varied at four levels and selected in a manner so that the revolution pitch could comprise both lower and higher magnitude of variation when compared among them. An attempt was made to investigate the material flow from the macrostructure of both vertical (transverse to welding direction) and horizontal (parallel to the weld surface) cross-section. The study showed a significant amount of variation in terms of spindle torque, forces, material flow, and tensile properties. The increased material flow was noticed in the top surface of the weld from advancing to the retreating side at increased revolution pitch. Whereas an increased material flow was observed in the downward direction through the retreating side of the nugget. At increased revolution pitch a clear division in the onion ring was noticed towards the retreating side. The variation of torque, force and material flow showed a consistent trend for a higher change in revolution pitch. As the revolution pitch increased finer nugget grains were obtained causing increased tensile properties.

Key-words: Friction stir welding; Revolution pitch; Material flow; Square tool.

1. Introduction

In 1991 Thomas et al. [1] developed the Friction stir welding at TWI to accomplish the joining of aluminum in solid-state. A rotating tool with a pin attached to a shoulder is fed in the interface of two plates to be joined and a traverse movement is provided to complete the welding. During this process, heat is contributed by the friction between the tool-workpiece boundary and severe plastic deformation of workpiece material. The deformation of the workpiece and material flow around the tool resulted in a generation of torque (spindle torque) and forces (Z-force, X-force). A spindle torque is the resistance of workpiece material against the angular deformation applied by the tool. Pew et al. [2] empirically developed a model of weld power and heat input from the torque for different grades of aluminum alloy. The model developed, successfully predicts the softening and enlargement of HAZ for AA7075. The Z-force and X-force are the resistances offered by the workpiece material to the vertical and traverse movement of the tool respectively. Trimble et al. [3] investigated tool forces both numerically and experimentally. They found during the initial plunge stage tool failures are likely to occur due to higher stresses. A variation in pin design can significantly alter the forces applied to the tool.

Andrade et al. [4] numerically developed a thermo-mechanical model to correlate the effect of the principal process parameters, tool dimensions, and plate thickness, on the torque and temperatures for FSW of varying grades of aluminum alloy (AA2xxx, AA5xxx, AA6xxx, and AA7xxx). They found that tool traverse speed has a strong dependency on plate thickness in terms of torque and temperature generated. They further observed that the temperature decreases with an increase in the product of traverse speed and plate thickness whereas an increase is observed for torque. They also developed a 'geometry parameter' (G) that corresponds to the effective contact area between tool-workpiece and found that with an increase in 'G' torque increases. It is inferred by Kumar [5] that an ultrasonic vibration-assisted friction stir welding can scale down the forces applied on the tool. Conferring to the review of Mishra et al. [6] online monitoring of these entities has the potential to control the weld quality during processing. Mishra et al. [7] have also experimentally shown the utility of the online monitoring of torque and forces by developing a cloud-based signal processing feedback system for quality monitoring of FSW from a remote location in real-time. Besides the heat transfer, the movement of plastically deformed workpiece material in the weldment is a vital issue. Several studies were made from different perspectives to unveil the phenomenon of material flow in FSW. Colligan [8] investigated the material flow for friction stir welding of aluminum by introducing tracer material in the joining line. He found that a large portion of the material

movement was dominated by the extrusion process. The material that went through the stirring action of pin primarily originated in the top section of the welds that flowed downward by the threads. Chen et al. [9] developed a numerical model to analyze the specialty of threaded pin tool. They found threaded tool results in an accelerated flow velocity and enhanced strain rate. They also observed several circular flow patterns around the tool pin due to its ability to trap the high-velocity material inside the thread and also creates a vertical pressure gradient which assists a better material flow from the top to bottom. Morisada et al. [10] attempted to track the material flow three-dimensionally by X-ray radiography using small globules of tungsten as a tracer. As the FSW process is being developed, another independent factor besides the machine process parameters (i.e. rotational speed, traverse speed, tilt angle, plunge depth, etc.) that attracts the researchers most is the tool design. In this context, several researchers have demonstrated different advantages for different tool designs. Fujii et al. [11] experimented the effectiveness of different tool designs for a range of aluminum alloys and concluded that the effectiveness of tool pin design is greatly affected by resistance to deformation of selected workpiece material. Jamshidi Aval et al. [12] investigated three different tool geometries with a combination of different tool pin shoulder design for dissimilar FSW (AA 5086-O and AA 6061-T6). They found that a tool with a concave shoulder and a conical pin with three grooves generates higher heat input and provides better stirring. Li et al. [13] tried to increase the thermal efficiency of the FSW process by incorporating new design features in the tool. They tried different tool features such as a hollow shank, fluted and thermally insulated tool to restrict the heat transfer to the tool. They found a rise in thermal efficiency by 4.2% and 14.1% for aluminum and steel respectively. Dialami et al. [14] developed a two-stage numerical process for analysis of material flow and related forces for circular, triflute, trivex, and triangular pin tools. They found that transverse forces are fairly less magnitude than longitudinal forces for all tools. For perfect stick condition, the heat generation and forces increase with an increase in pin area. However, no significant difference is observed in temperature field, strain rate, and streamlines for varying pin shapes. Contrary to this for perfect slip condition pin shapes are found to have a strong influence on strain rate and streamlines. The sharp corners and segments contributed to heat generation and material flow. Elangovan and Balasubramanian [15,16] found that among the five different tool-pin designs, square pin produced sound welds in terms of mechanical and metallurgical properties for AA 2219 with varying tool rotational speed and traverse speed. In two different studies for AA 6061, Elangovan et al. [17,18] noticed that a square tool yielded defect-free welds irrespective of applied axial force and shoulder diameter. Palanivel et al. [19] have also obtained the highest tensile strength with the square pin tool for dissimilar FSW. Other than the similar or dissimilar aluminum alloy FSW square pin tool is found to be promising with metal matrix composites also. Vijay and Murugan [20] reported a finer distribution of reinforced particles due to pulsating stirring action for Al–10 wt.% TiB_2 metal matrix composites. Due to similar pulsating stirring action for friction stir processing Mahmoud et al. [21] reported a uniform distribution of SiC particles on the surface layer of AA1050-H24 plates. Mugada and Adepu [22] observed that polygonal pins reduced the plunge force at the initial stage of welding owing to pulsating stirring action for FSW of AA 6082. They alsoachieved an adequate mixing and circulation of material in both advancing and retreating side for square tool with superior mechanical properties. Mehta et al. [23] developed a numerical model by utilizing the principle of orthogonal machining for the estimation of frictional heat for different polygonal tools. They further utilized the figured thermal data from the numerical model for the estimation of the torque, traverse force, and the mechanical stresses acting on the polygonal tools. They concluded that the peak temperature had a directly proportional relationship with the number of flat faces of the tool whereas for the shear stress it was observed to be opposite. Malik and Kailas [24] devised an interesting experiment using plasticine modeling of material mixing for FSW. Plasticine of different colors was used and the intensity of the final color was analyzed to assess the extent of mixing for different polygonal tools. For higher weld pitch, they found an increased amount of material spin in a single revolution of the tool. Whereas with an increased number of flat faces of the tool, the amount of material that spins reduced.

Besides the study of sole individual process parameters, researchers also devoted their concern regarding the combined effect of more than one parameter at a time. For such studies, weld pitch and revolution pitch are the two factors that researchers often refer to. Weld pitch is obtained by dividing the tool rotational speed with tool traverse speed (N/V) i.e. the number of tool rotations for a unit length of tool movement. Gharacheh et al. [25] studied the effect of weld pitch on mechanical properties of FSWedMg alloy. Seidel and Reynolds [26] stressed the reciprocal of weld pitch (V/N) that is revolution pitch to address the material flow issues. For a dissimilar lap joint (AA6111-T4 and AA5023-T4) Park et al. [27] analyzed the effect of weld pitch and shoulder diameter on tensile shear load. They found that as the weld pitch decreases the interface changed to a flat shape from a hooked pattern. The shoulder diameter and weld pitch significantly altered the fractured area. For AA 6061-T6 joints Liu et al. [28] found that beyond an optimum revolution pitch the tensile properties degraded and fractured in nugget because of serious softening and crack formation.

Considering the revolution pitch as a parameter one can reduce the number of parameters to be studied. It can also readily give a comparative idea about the heat input and material processed. Most of the literature available for friction stir welding primarily deals with each process parameter individually for different analyses. Moreover, for the square tool, the study of revolution pitch on AA 6061-T6 is farther a rare combination.

2. Experimental Detail

6 mm thick plate of AA 6061-T6 in square but configuration was used in this present study. The tool selected for the purpose was a square pin tool (four sides are flat) made of H13 tool steel with 5.6 mm pin height, diagonal of the square pin was 6 mm. The shoulder diameter was kept at 18 mm and a 5° concavity was provided (Figure 1). In this study, four different sets of welding were conducted for an effective welding length of 120 mm on AA 6061-T6 (120 mm×6.5 mm×6mm). The four different weldings were carried out at constant Z-axis position by considering the variation of tool rotational speed and traverse speed (tilt angle of 2°) to produce a significant variation in tool revolution pitch. The values of the parameters were chosen through the trial-and-error method (Table 1). Two different strain gauge-based load cells were employed, (one on machine carriage and another at spindle head) connected with the PLC system and NI LabVIEW software to capture the generated spindle torque, Z-force, and X-force. The whole setup for capturing the torque and forces is inbuilt in the FSW machine. The Z and X-axis thrust capacity of the machine is 30 KN and 10 KN (Maximum). The torque and forces were considered from the starting of the tool traverse. For each welding time-temperature profile was considered in the advancing side (in the middle of the weld length)at 12 mm distance from the middle of nugget and 3 mm depth along the plate thickness using a K-type thermocouple. For macro and microstructural analysis specimens were prepared by polishing with several grades of emery paper, diamond paste and finally etching was done with Keller's reagent. To analyze the material flow and weld formation, macrostructures of both vertical and horizontal cross-sections were considered. A light optical microscope was employed for the determination of nugget grain size. ASTM-E8 standard was followed for the preparation of tensile samples and an Instron 8801 with a strain rate of 1 mm sec^{-1} was used for tensile tests. Scanning electron microscopy was also used for fractographic analysis.

Table 1. Process parameters setting and respective revolution pitch, pulse per mm.

Sl. No.	Rotational Speed (rpm) (N)	Traverse Speed (mm/sec) (V)	Revolution Pitch (mm/rev) (R.P)	Tool Pulse/Sec (Hz)	Tool Pulse/mm
1.	1100	2.25	0.122	73.33	32.59
2.	900	1.75	0.116	60.00	34.28
3.	1500	1.25	0.054	100.00	80.00
4.	1300	0.75	0.034	86.66	115.54

Figure 1. Square pin tool.

3. Results and Discussion

3.1. Analysis of spindle torque and different forces:

From Figure 2 it can be recognized that at higher revolution pitches (0.116 mm/rev and 0.122 mm/rev) the distribution of spindle torque is more stable (Figure 2a). Whereas, for lower revolution pitches as the tool proceeds a fluctuation in spindle torque can be seen. Further for lower revolution pitches the extent of the fluctuation is comparatively more at 0.034 mm/rev than 0.054 mm/rev. A similar kind of observation can be made for Z-force at 0.054 mm/rev and 0.034 mm/rev (Figure 2b). From Figure 2c it can be noticed that the fluctuation for X-force in case of 0.034 mm/rev and 0.054 mm/rev is far less than 0.116 mm/rev and 0.122 mm/rev. The fluctuation of X-force indicates the difference in the degree of plastic deformation between the advancing and retreating sides as the heat input and material flow differ on both sides. Kadian and Biswas [29] found different degrees of deformation and temperature variation between the advancing and retreating sides for different tool geometries.

Lower revolution pitches (0.034 mm/rev and 0.054 mm/rev) possesses a larger tool interaction time than higher revolution pitches (0.116 mm/rev and 0.122 mm/rev). Whereas, the pulse generated per unit length at higher revolution pitches is lesser in comparison to lower revolution pitches (Table 1). All these conditions lead to a higher order of plastic deformation and higher peak temperatures (Figure 3) for lower revolution pitches. Again from Figure 2c, it can be observed that at 0.054 mm/rev the fluctuation of X-force reduces drastically than 0.034 mm/rev through the interaction time is less. At 0.054 mm/rev the frequency of the pulse is highest among all (100 pulses/sec, Table 1) which shows the material around the tool is subjected to the highest number of pulsating actions per unit time. This indicates a higher as well as more uniform deformation in both advancing and retreating sides is achieved as the tool has to rotate fast causing such a drastic decrease in X-force fluctuation. Again from Figure 2d, it can be observed that at lower revolution pitch the need for generated spindle torque and forces (X-force, Z-force) are appreciably less and can be attributed to the higher deformation of the workpiece. Such conditions may rise to the occurrence of a slipping phenomenon between the tool-workpiece interface resulting in a disturbance in spindle torque and Z-force distribution at lower revolution pitch (Figure 2a, b). Qian et al. [30] stated the variation of torque and force fluctuation in FSW is related to the stick-slip contact condition that exists in tool-workpiece interphase.
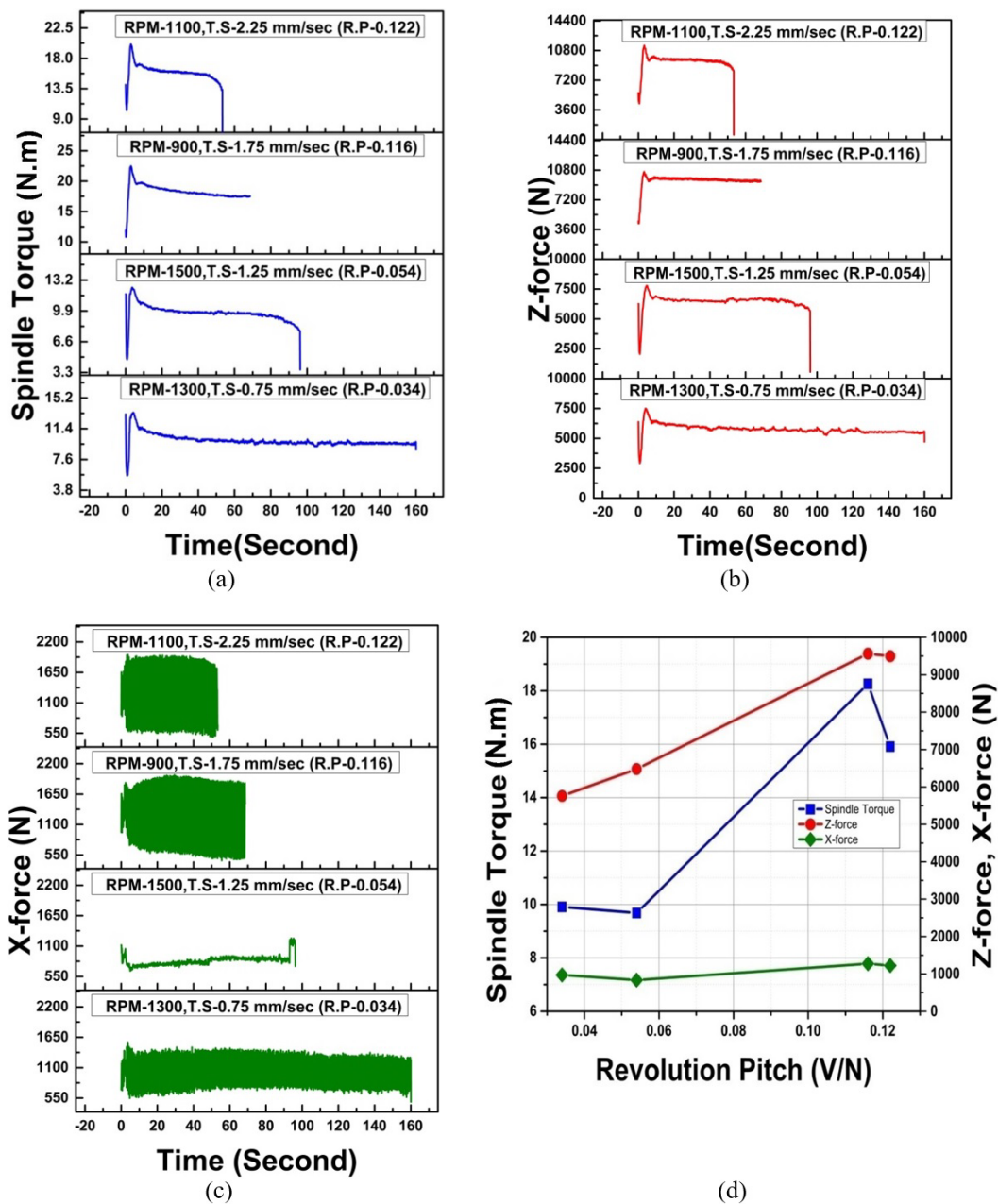
Figure 2. (a) Variation of spindle torque with time; (b) Variation of Z-force with time; (c) Variation of X-force with time; (d) Average spindle torque, Z-force and X-force for varying revolution pitch.
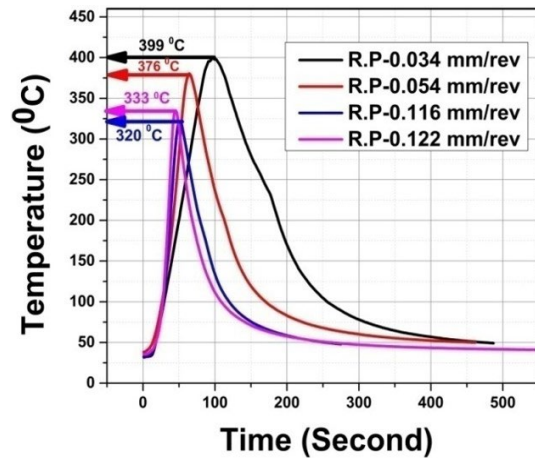
Figure 3. Time-temperature plot for each welding.

3.2. Weld formation

Figure 4 represents the weld macrostructure of horizontal cross-sections at a depth of 1 mm approximately for all the welds. In the horizontal cross-section of all the welds, a line can be seen roughly at some offset distance from the middle of the nugget that continues along the welding direction. Colligan [8], in his study of material flow behavior during FSW of Al alloy by radiographic analysis, observed reorientation of steel balls at the faying surface (steel balls used for material flow tracking in the faying surface) roughly in a line in the same fashion that is observed in Figure 4. The continuous line of steel shots was reoriented behind the tool as the material from the front of the tool during welding (from the advancing side) passes across it and consolidates behind the tool on the retreating side. It can be noticed that almost all the lines in Figure 4 are at an offset distance from the center of the weld longitudinal axis towards the retreating side. This offset distance indicates how far the material, sheared by the tool from the advancing side, has traveled to the retreating side before it consolidates below the shoulder and appeared as in the form of a line. It is seen that the offset distance is increasing with an increase in revolution pitch. At the lowest revolution pitch of 0.034 mm/rev, it is 0.5 mm and the highest offset distance is 2.31 mm for 0.122 mm/rev.
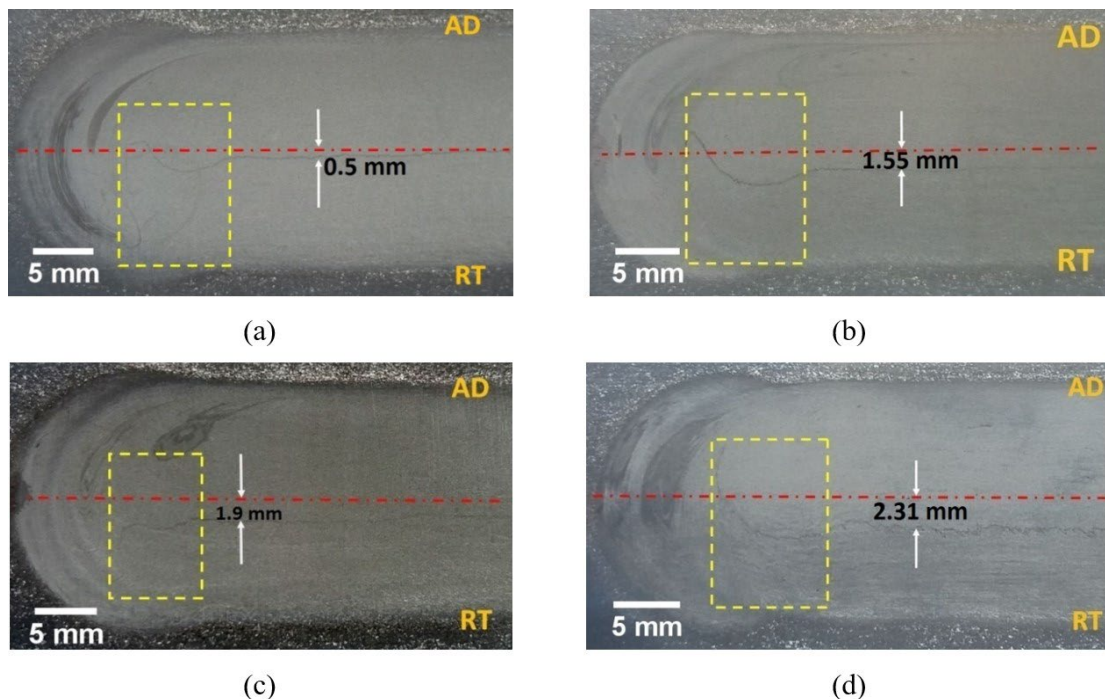
Figure 4. Macrostructure of horizontal cross-section at 1mm depth (a) 0.034 mm/rev; (b) 0.054 mm/rev; (c) 0.116 mm/rev; (d) 0.122 mm/rev (AD: Advancing side, RT: Retreating side).

It depicts a better material mixing is achieved between advancing and retreating sides with an increase in revolution pitch. At higher revolution pitch the material is comparatively less deformed, which reduces the occurrence of slipping of

deformed material around the tool. As a result, a better gripping between the tool and deformed material may have achieved causing such increased advancement of deformed material towards the retreating side under the shoulder.

From the vertical cross-sections of the nugget, it can be observed that the onion rings are comparatively large at the lower revolution pitch (Figure 5, 6a). It indicates at lower revolution pitches, due to increased interaction and number of pulse per second, the effect of the pin is more dominant, than higher revolution pitches. Whereas, at higher revolution pitches (0.116 and 0.122 mm/rev) the size of the onion ring is relatively small but more distinct and the shoulder induced region is comparatively large than lower revolution pitches. It indicates that, as the interaction time between tool and workpiece reduces the shoulder induced flow becomes more dominant over the pin induced flow. The distinct division in the onion ring pattern shows an increased downward material flow from the shoulder at the retreating side causing an interaction of material flows that are moving in different directions. This may cause the generation of localized material flow in the interface resulting in a division in the onion ring.
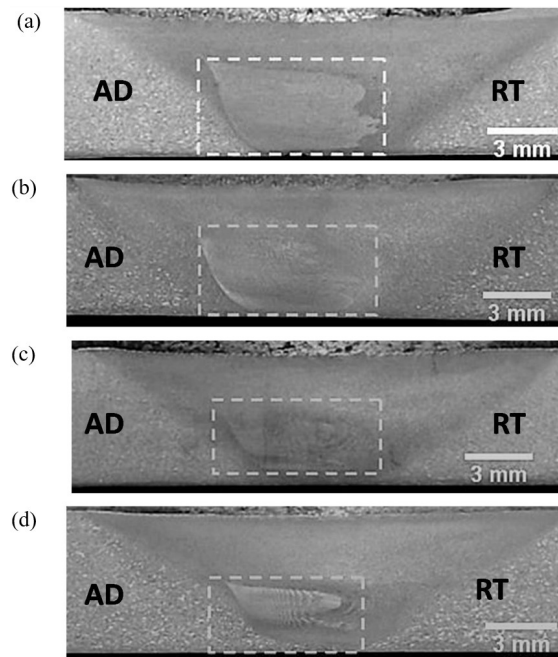
Figure 5. Macrostructure of vertical cross section (a) 0.034 mm/rev; (b) 0.054 mm/rev; (c) 0.116 mm/rev; (d) 0.122 mm/rev.
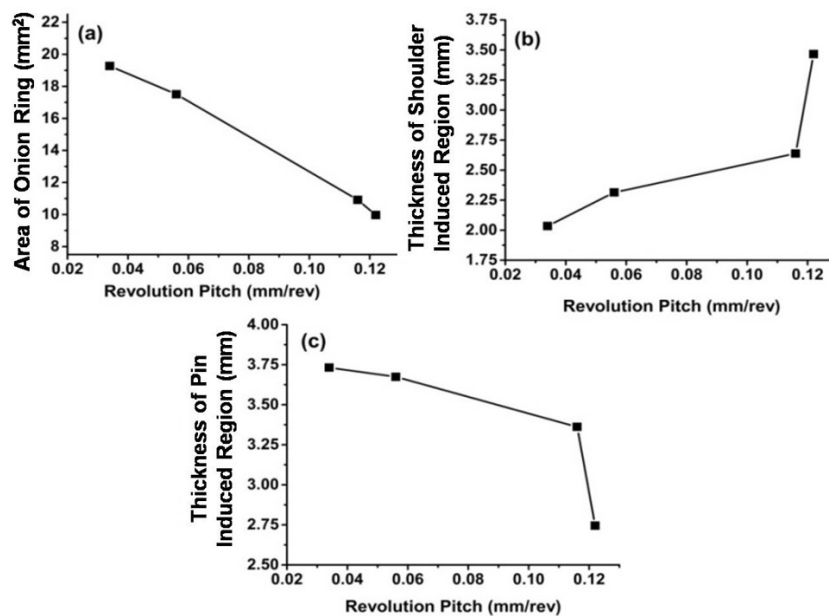
Figure 6. (a) Variation of onion ring area (b) Variation of shoulder induced region (c) Variation of pin induced region.

Figure 7 represents the horizontal cross-section of the exit hole macrostructure at a depth of 1 mm. It can be observed that at lower revolution pitch the surrounding of the exit hole is evenly distributed with deformed material (Figure 7a, b) in both advancing and retreating. Whereas, at increased revolution pitch (Figure 7c) the material flow around the exit hole in the advancing side is less. This causes a discontinuity of the material flow around the exit hole from the advancing side of the exit hole. With a further increase in revolution pitch to 0.122 mm/rev (Figure 7d), the material in the advancing side of the nugget stops much ahead of the exit hole. Moreover, the joining line gets distorted 4.3 mm and 4.7 mm away from the boundary of the exit hole at 0.032 mm/rev and 0.116 mm/rev respectively (Figure 7a, c). At increased revolution pitch the tool has to pass over an increased length for a single rotation and thus tool has to process more material. Hence, an increase in material flow from advancing to the retreating side may happen. But the deposition from retreating to the advancing side beneath the shoulder is reduced and is evident as the material flow is increasingly discontinued ahead of the exit hole in the advancing side with an increase in revolution pitch. Hence it is an indication that this increased material flow from the advancing to the retreating side below the shoulder must be accommodated by the weld nugget to maintain the continuity of the material flow. Liu and Wu [31], also have observed an increased downward flow of material in case of material in retreating side increases and the reason they attributed is the conservation of mass within the nugget. Accordingly from the vertical cross-section of nugget (Figure 5d, 6b, c), it is seen that the pin induced regions are small in size than the shoulder induced region. Also, the advancement of the onion ring towards the retreating side of the nugget is dominated by the material continuing from the shoulder induced region (Figure5c,d). This indicates that at a higher revolution pitch the downward material flow is more. Also, the division of the onion ring indicates the occurrence of localized material flow in the bottom portion of the weld (Figure 5c, d). All these together point towards a better mixing of deformed material at a higher revolution pitch even at the bottom of the weld.
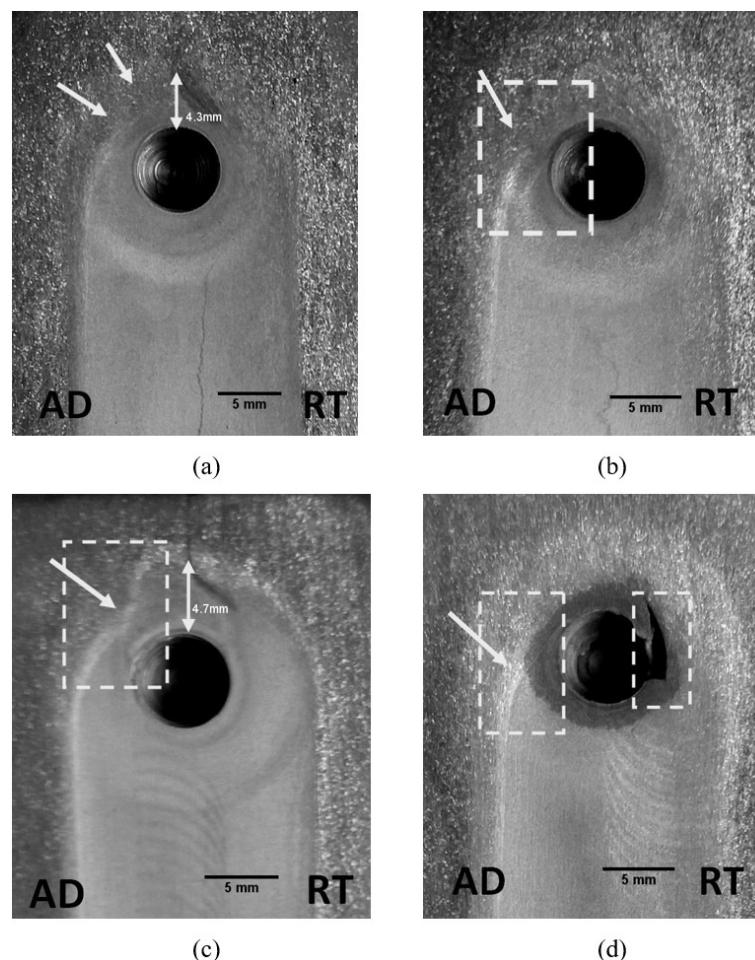
Figure 7. Horizontal cross section of exit hole macrostructure at a depth of 1 mm (a) 0.034 mm/rev; (b) 0.054 mm/rev; (c) 0.116 mm/rev; (d) 0.122 mm/rev.

3.3. Analysis of nugget grain

The grains of the base material are elongated due to rolling operation whereas, the nugget zone of all the weldings encountered equiaxed grains due to dynamic recrystallization (Figure 8). From Figure 8 and Table 2 it can be observed that finer grains in the nugget zone are evident at higher revolution pitches (0.116 mm/rev and 0.122 mm/rev). The amount of heat

generation, rate of cooling, and degree of deformation during welding contributes to the size of nugget grain. An increased heat generation can provide better deformation of the workpiece, however, at the same time, it can reduce the cooling rate. Exposure to a lower cooling rate or higher heat can cause grain growth due to higher nucleation time. A higher heat generation will eventually rise to the size of nugget grains due to slower cooling as friction stir welding is a comparatively slower welding process. Zhang et al. [32] found an increase in temperature by means of increased rotational speed or shoulder diameter can increase the nucleation rate to many folds and thereby increased grain size in nugget. At a higher revolution pitch, finer grains are obtained as the heat source (tool) has to move through an increased amount of material for a single revolution. In other words, the tool moves faster, resulting in lower heat input (Table 3), lower peak temperature, and increased cooling rate (Figure 3). Whereas, at lower revolution pitch the interaction between the tool and workpiece is more than higher revolution pitch causing a higher heat input. It can be ascertained from the heat input (Table 3) for each welding that is calculated from Equation 1 and 2 [33,34].

Table 2. Variation of Avg. grain size with revolution pitch and the base material along the rolling direction.

Revolution pitch (mm/rev)	0.034	0.054	0.116	0.122	Base Material
Avg. Grain Diameter (μm)	12.8	8.6	7.14	7.62	51.74
Standard deviation (±)	1.43	0.6	0.46	0.99	10.53

Table 3. Variation of friction coefficient and heat input with revolution pitch.

Revolution Pitch (mm/rev)	0.034	0.054	0.116	0.122
Friction Coefficient (μ)	0.287	0.251	0.319	0.283
Heat Input (Joule)	1800	1216	983	814
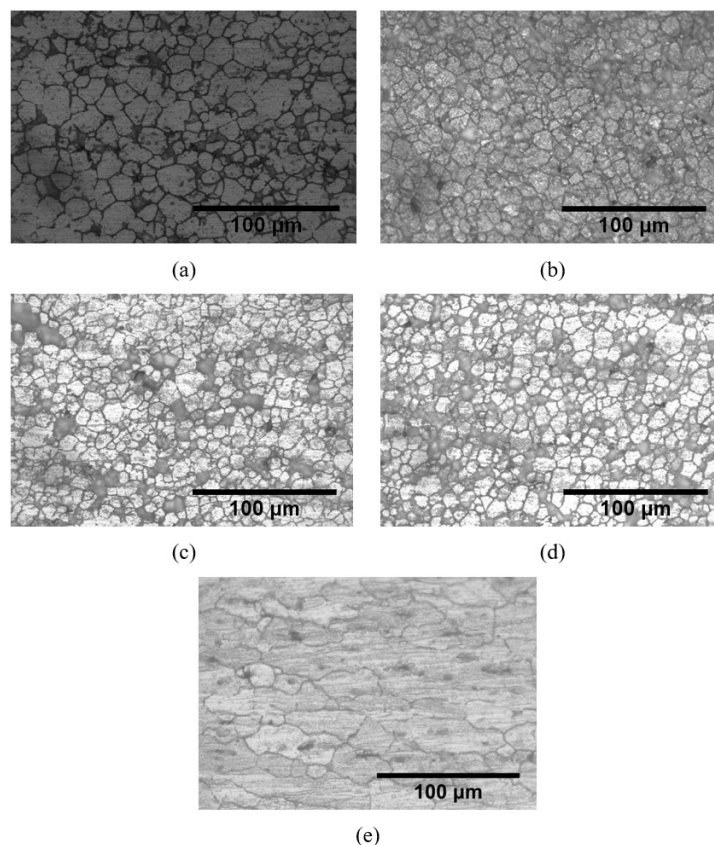
Figure 8. Distribution of grain size in nugget zone for different revolution pitches (a) 0.034 mm/rev; (b) 0.054 mm/rev; (c) 0.116 mm/rev; (d) 0.122 mm/rev; (e) Base material.

$$\mu = \frac{3T}{DN}$$

(1)

where, T=Torque, P=Contact Pressure, D=2R (Tool radius), N=Normal Pressure, μ=Friction coefficient

$$Q = \frac{2}{3}\mu\omega\frac{F}{vR_s^2}\left[\left(R_s^3 - R_p^3\right)(1 + tan\alpha) + R_p^3 + 3R_p^2 H_p\right] \tag{2}$$

where, Q (kJ/mm) is heat input, μ is friction coefficient, ω is the angular velocity of tool (rad/sec), F (KN) is axial load, v (mm/sec) is traverse speed, R_s (m)is shoulder diameter, R_p (m) is pin diameter, H_p (m) is pin height, α (degree)concavity of shoulder.

3.4. Analysis of tensile properties

Figure 9 represents the tensile properties considered along the transverse of the welding for varying revolution pitches. It can be noticed that the revolution pitch has a prominent effect on tensile properties. As revolution pitch is increasing the overall tensile properties are also increasing. The highest tensile strength is 248.48 MPa at 0.122 mm/rev and the lowest is 194.97 MPa at 0.034 mm/rev (Table 4). However, a decrease in tensile properties than the base material is observed for all welded samples. This is a common phenomenon seen for FSW of Al alloys and is caused by the dissolution of strengthening particles in the nugget. From Figure 2d it is noticed that at higher revolution pitch increased torque and Z-forces are achieved resulting in improved material flow (Figure 4d, 5d). Also at a higher revolution pitch, finer grains are achieved. All these together support the observations of improved tensile properties at higher revolution pitch.
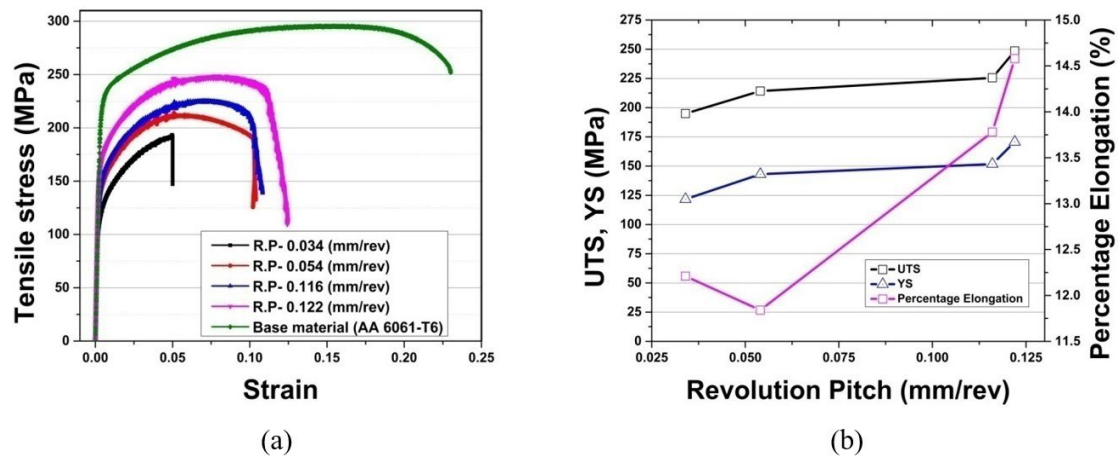
Figure 9. Tensile properties for different revolution pitches (a) stress vs strain for different revolution pitches; (b) UTS, YS, percentage elongation for different revolution pitches.

Table 4. Variation of tensile properties with revolution pitch.

Revolution Pitch (mm/rev)	UTS (MPa)	YS (MPa)	Percentage Elongation (%)
0.034	194.97	121.68	12.21
0.054	214.18	143.09	11.84
0.116	225.52	151.79	13.78
0.122	248.48	170.70	14.58
Base Material	295.23	255.50	17.80

3.5. Fractography

A substantial variation in fracture characteristics is observed (Figure 10) with variation in revolution pitch in terms of fracture position and surface characteristics. Almost all the samples fractured at the outside of the nugget zone towards the advancing side of the weld (except the specimen at 0.122 mm/rev) with a significant proportion of deformation. This may be caused by the higher heat generation at the advancing side, which often weakens the microstructure due to grain coarsening and dissolution of precipitates. However, at the highest revolution pitch of 0.122 mm/rev, an exception is observed with a fracture in the retreating side of the weld (Figure 10d). At higher revolution pitch the tool-workpiece interaction is reduced significantly. This may lead to a situation where comparatively a lesser dissolution of strengthening particles happens with finer grains on the advancing side. Moreover, as discussed earlier the material flow from the retreating to advancing side is more at 0.122 mm/rev and the opposite is also true (Figure 4,5). This also may contribute to the change of fracture location from the advancing to the retreating side. A higher deformation in fractured samples indicates all the samples have gone through a ductile fracture, which is also evident from the observation of dimple-shaped voids in all the fractured samples (Figure 10e-h). However, at a lower revolution pitch of 0.032 mm/rev, the dimples are large and elongated (Figure 10e) and

are characterized by the lowest tensile strength (Figure 9). With an increase in revolution pitch, the dimples are becoming smaller. At 0.122 mm/rev the fractured surface is characterized by finer dimples (Figure 10h) and has attained the highest strength (Figure 9) under tensile loading.
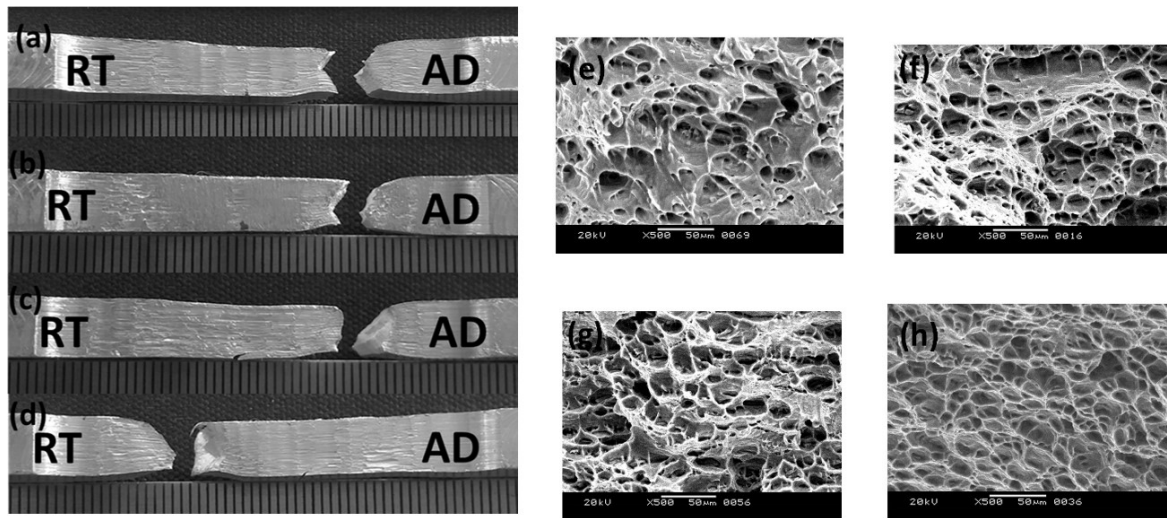
Figure 10. Variation of fracture position and fracture surface for varying revolution pitch (a, e) 0.034 mm/rev, (b,f) 0.054 mm/rev, (c,g) 0.116 mm/rev, (d,h) 0.122 mm/rev.

4. Conclusions

1. At a higher revolution pitch (0.122 mm/rev and 0.116 mm/rev) the distribution of spindle torque is more stable. Whereas, for lower revolution pitches (0.034 mm/rev than 0.054 mm/rev) a more fluctuation in spindle torque and Z-force is observed. For lower revolution pitches, the fluctuation of X-force is far less than higher revolution pitches. At lower revolution pitch the spindle torque, Z-force, and X-force are substantially low;

2. At 0.054 mm/rev the fluctuation of X-force shows a drastic reduction and can be attributed to the highest number of pulse frequency (100 pulses/sec) attained by the tool at that revolution pitch;

3. From the macrostructure of horizontal cross-section, a formation of a line can be seen with an increasing offset distance from the center of the weld line with an increase in revolution pitch;

4. In the exit hole region (Horizontal cross-section) at the lower revolution pitch, an even spread of deformed material on both advancing and retreating sides can be observed. Whereas, at increased revolution pitch the deformed material does not continue around the exit hole;

5. Both the increased offset distance of midline towards retreating side and discontinuation of material flow around the exit hole in the advancing side depicts increased material flow from advancing to retreating side as well as in downward direction at higher revolution pitch. It can be confirmed from the increased Z-force, higher shoulder induced material flow from the retreating side at 0.116 mm/rev and 0.122 mm/rev;

6. The onion rings are comparatively larger at the lower revolution pitch. Whereas at higher revolution pitch (0.116 and 0.122 mm/rev) the onion ring size is less, and the shoulder induced region is more with distinct onion ring pattern. A prominent division in the onion ring pattern is observed at 0.116 mm/rev and 0.122 mm/rev depicting a form of localized flow;

7. For a higher change of revolution pitch (as 0.054 mm/rev to 0.116 mm/rev) the observation in terms of torque, forces, and material flow are more prominent than a smaller change in revolution pitch (as 0.034 mm/rev to 0.054 mm/rev and 0.116 mm/rev to 0.122 mm/rev);

8. At increased revolution pitch, the nugget grains become finer due to less heat input and a higher cooling rate. The maximum and minimum grain diameter achieved is 12.8 μm and 7.14 μm at 0.034 mm/rev and 0.116 mm/rev respectively;

9. All the samples fractured outside the nugget zone except for the 0.122 mm/rev (outside the nugget zone on the retreating side). As the revolution pitch increases, the tensile strength improves. The maximum and minimum tensile strength is 194.97 MPa and 248.48 MPa at 0.034 mm/rev and 0.122 mm/rev respectively.

References

[1] Thomas WM, Nicholas ED, Needham JC, Murch MG, Temple-Smith P, Dawes CJ. International patent application PCT/GB92/02203 and GB patent application 9125978.8. Psychiatric Bulletin. 1991;15(12):778. http://dx.doi.org/10.1192/pb.15.12.778.

[2] Pew JW, Nelson TW, Sorensen CD. Torque-based weld power model for friction stir welding. Science and Technology of Welding and Joining. 2007;12(4):341-347. http://dx.doi.org/10.1179/174329307X197601.

[3] Trimble D, Monaghan J, O'Donnell GE. Force generation during friction stir welding of AA2024-T3. CIRP Annals. 2012;61(1):9-12. http://dx.doi.org/10.1016/j.cirp.2012.03.024.

[4] Andrade DG, Leitão C, Dialami N, Chiumenti M, Rodrigues DM. Modeling torque and temperature in friction stir welding of aluminium alloys. International Journal of Mechanical Sciences. 2020;182:105725. http://dx.doi.org/10.1016/j.ijmecsci.2020.105725.

[5] Kumar S. Ultrasonic-assisted friction stir processing of 6063 aluminum alloy. Archives of Civil and Mechanical Engineering. 2016;16(3):473-484. http://dx.doi.org/10.1016/j.acme.2016.03.002.

[6] Mishra RS, Ma ZY. Friction stir welding and processing. Materials Science and Engineering R Reports. 2005;50(1-2):1-78. http://dx.doi.org/10.1016/j.mser.2005.07.001.

[7] Mishra D, Gupta A, Raj P, Kumar A, Anwer S, Pal SK, et al. Real time monitoring and control of friction stir welding process using multiple sensors. CIRP Journal of Manufacturing Science and Technology. 2020;30:1-11. http://dx.doi.org/10.1016/j.cirpj.2020.03.004.

[8] Colligan K. Material flow behavior during friction welding of aluminum. Welding Journal. 1999;75:229s-237s.

[9] Chen G, Li H, Wang G, Guo Z, Zhang S, Dai Q, et al. Effects of pin thread on the in-process material flow behavior during friction stir welding: a computational fluid dynamics study. International Journal of Machine Tools & Manufacture. 2018;124:12-21. http://dx.doi.org/10.1016/j.ijmachtools.2017.09.002.

[10] Morisada Y, Fujii H, Kawahito Y, Nakata K, Tanaka M. Three-dimensional visualization of material flow during friction stir welding by two pairs of X-ray transmission systems. Scripta Materialia. 2011;65(12):1085-1088. http://dx.doi.org/10.1016/j.scriptamat.2011.09.021.

[11] Fujii H, Cui L, Maeda M, Nogi K. Effect of tool shape on mechanical properties and microstructure of friction stir welded aluminum alloys. Materials Science and Engineering A. 2006;419(1-2):25-31. http://dx.doi.org/10.1016/j.msea.2005.11.045.

[12] Jamshidi Aval H, Serajzadeh S, Kokabi AH, Loureiro A. Effect of tool geometry on mechanical and microstructural behaviours in dissimilar friction stir welding of AA 5086--AA 6061. Science and Technology of Welding and Joining. 2011;16(7):597-604. http://dx.doi.org/10.1179/1362171811Y.0000000044.

[13] Li H, Gao J, Li Q, Galloway A, Toumpis A. Effect of friction stir welding tool design on welding thermal efficiency. Science and Technology of Welding and Joining. 2019;24(2):156-162. http://dx.doi.org/10.1080/13621718.2018.1495868.

[14] Dialami N, Cervera M, Chiumenti M, Saracibar CA. A fast and accurate two-stage strategy to evaluate the effect of the pin tool profile on metal flow, torque and forces in friction stir welding. International Journal of Mechanical Sciences. 2017;122:215-227. http://dx.doi.org/10.1016/j.ijmecsci.2016.12.016.

[15] Elangovan K, Balasubramanian V. Influences of pin profile and rotational speed of the tool on the formation of friction stir processing zone in AA2219 aluminium alloy. Materials Science and Engineering A. 2007;459(1-2):7-18. http://dx.doi.org/10.1016/j.msea.2006.12.124.

[16] Elangovan K, Balasubramanian V. Influences of tool pin profile and welding speed on the formation of friction stir processing zone in {AA}2219 aluminium alloy. Journal of Materials Processing Technology. 2008;200(1-3):163-175. http://dx.doi.org/10.1016/j.jmatprotec.2007.09.019.

[17] Elangovan K, Balasubramanian V, Valliappan M. Influences of tool pin profile and axial force on the formation of friction stir processing zone in AA6061 aluminium alloy. International Journal of Advanced Manufacturing Technology. 2008;38(3-4):285-295. http://dx.doi.org/10.1007/s00170-007-1100-2.

[18] Elangovan K, Balasubramanian V, Valliappan M. Effect of tool pin profile and tool rotational speed on mechanical properties of friction stir welded AA6061 aluminium alloy. Materials and Manufacturing Processes. 2008;23(3):251-260. http://dx.doi.org/10.1080/10426910701860723.

[19] Palanivel R, Mathews PK, Murugan N, Dinaharan I. Effect of tool rotational speed and pin profile on microstructure and tensile strength of dissimilar friction stir welded AA5083-H111 and AA6351-T6 aluminum alloys. Materials & Design. 2012;40:7-16. http://dx.doi.org/10.1016/j.matdes.2012.03.027.

[20] Vijay SJ, Murugan N. Influence of tool pin profile on the metallurgical and mechanical properties of friction stir welded Al--10 wt.% TiB2 metal matrix composite. Materials & Design. 2010;31(7):3585-3589. http://dx.doi.org/10.1016/j.matdes.2010.01.018.

[21] Mahmoud ERI, Takahashi M, Shibayanagi T, Ikeuchi K. Effect of friction stir processing tool probe on fabrication of SiC particle reinforced composite on aluminium surface. Science and Technology of Welding and Joining. 2009;14(5):413-425. http://dx.doi.org/10.1179/136217109X406974.

[22] Mugada KK, Adepu K. Influence of ridges shoulder with polygonal pins on material flow and friction stir weld characteristics of 6082 aluminum alloy. Journal of Manufacturing Processes. 2018;32:625-634. http://dx.doi.org/10.1016/j.jmapro.2018.03.034.

[23] Mehta M, Reddy GM, Rao AV, De A. Numerical modeling of friction stir welding using the tools with polygonal pins. Def Technol. 2015;11(3):229-236. http://dx.doi.org/10.1016/j.dt.2015.05.001.

[24] Malik V, Kailas SV. Plasticine modeling of material mixing in friction stir welding. Journal of Materials Processing Technology. 2018;258:80-88. http://dx.doi.org/10.1016/j.jmatprotec.2018.03.008.

[25] Gharacheh MA, Kokabi AH, Daneshi GH, Shalchi B, Sarrafi R. The influence of the ratio of "rotational speed/traverse speed"(ω/v) on mechanical properties of AZ31 friction stir welds. International Journal of Machine Tools & Manufacture. 2006;46(15):1983-1987. http://dx.doi.org/10.1016/j.ijmachtools.2006.01.007.

[26] Seidel TU, Reynolds AP. Visualization of the material flow in AA2195 friction-stir welds using a marker insert technique. Metallurgical and Materials Transactions. A, Physical Metallurgy and Materials Science. 2001;32(11):2879-2884. http://dx.doi.org/10.1007/s11661-001-1038-1.

[27] Park S-W, Yoon T-J, Kang C-Y. Effects of the shoulder diameter and weld pitch on the tensile shear load in friction-stir welding of AA6111/AA5023 aluminum alloys. Journal of Materials Processing Technology. 2017;241:112-119. http://dx.doi.org/10.1016/j.jmatprotec.2016.11.007.

[28] Liu H, Fujii H, Maeda M, Nogi K. Tensile properties and fracture locations of friction-stir welded joints of 6061-T6 aluminum alloy. Journal of Materials Science Letters. 2003;22(15):1061-1063. http://dx.doi.org/10.1023/A:1024970421082.

[29] Kadian AK, Biswas P. Effect of tool pin profile on the material flow characteristics of {AA}6061. Journal of Manufacturing Processes. 2017;26:382-392. http://dx.doi.org/10.1016/j.jmapro.2017.03.005.

[30] Qian JW, Li JL, Xiong JT, Zhang FS, Li WY, Lin X. Periodic variation of torque and its relations to interfacial sticking and slipping during friction stir welding. Science and Technology of Welding and Joining. 2012;17(4):338-341. http://dx.doi.org/10.1179/1362171812Y.0000000001.

[31] Liu XC, Wu CS. Material flow in ultrasonic vibration enhanced friction stir welding. Journal of Materials Processing Technology. 2015;225:32-44. http://dx.doi.org/10.1016/j.jmatprotec.2015.05.020.

[32] Zhang Z, Wu Q, Grujicic M, Wan ZY. Monte Carlo simulation of grain growth and welding zones in friction stir welding of AA6082-T6. Journal of Materials Science. 2016;51(4):1882-1895. http://dx.doi.org/10.1007/s10853-015-9495-x.

[33] Kumar K, Kalyan C, Kailas SV, Srivatsan TS. An investigation of friction during friction stir welding of metallic materials. Materials and Manufacturing Processes. 2009;24(4):438-445. http://dx.doi.org/10.1080/10426910802714340.

[34] Schmidt H, Hattel J, Wert J. An analytical model for the heat generation in friction stir welding. Modelling and Simulation in Materials Science and Engineering. 2004;12(1):143-157. http://dx.doi.org/10.1088/0965-0393/12/1/013.